Available online at www.sciencedirect.com

ScienceDirect

journal homepage: www.elsevier.com/locate/he

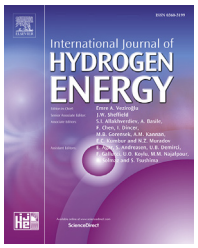

Energy management control design for fuel cell hybrid electric vehicles using neural networks

Pedro M. Muñoz [a,b], Gabriel Correa [c,*], Marcos E. Gaudiano [d], Damián Fernández [d]

[a] Universidad Nacional de Córdoba, Facultad de Ciencias Exactas, Físicas y Naturales, Av.Velez Sarsfield 1611, X5016GCA, Córdoba, Argentina

[b] INFIQC, Facultad de Ciencias Químicas, Universidad Nacional de Córdoba, CONICET, Ciudad Universitaria, 5000, Córdoba, Argentina

[c] CONICET – CITCA, Universidad Nacional de Catamarca – FACEN, Prado 366, K4700BDH, San Fernando del Valle de Catamarca, Argentina

[d] CIEM, CONICET & FaMAF, Universidad Nacional de Córdoba, Ciudad Universitaria, X5000HUA, Córdoba, Argentina

ARTICLE INFO

Article history:
Received 21 June 2017
Received in revised form
28 September 2017
Accepted 29 September 2017
Available online 26 October 2017

Keywords:
Fuel cell hybrid electric vehicle
Energy management system controller
Dynamic PEM fuel cell model
Hydrogen consumption minimization
Neural networks

ABSTRACT

The design and optimization of hybrid electric vehicle powertrains can take a great benefit from mathematical models which include auxiliary management and control strategies of the energy fluxes: the use of virtual platforms reduces the expensive and time-consuming experimental activity. In this work the authors developed an online Energy Management System (EMS) controller for a FCHEV, designed to employ the same energy management over a wide range of driving style types. The controller was designed by using neural networks (NN), which were trained with the optimal power flux distribution between a fuel cell system and a battery system that minimizes the overall equivalent energy consumption. The optimal solution was obtained by carrying out a gradient-based method minimization over eight different driving cycles, and using a dynamic lumped parameter mathematical model of a FCHEV fed by hydrogen and Li-ion batteries. A quantitative and qualitative analysis was made showing the networks performances over different type of cycles. Through this analysis, a suitable classification into two cycle categories is provided, covering most of the possible driving styles with two of the developed controllers.

Introduction

Currently, new and rapidly emerging hydrogen based technologies are being extensively used for propulsion systems of hybrid electric vehicles. Fuel Cell System (FCS) could become the main power source of electric vehicles in the forthcoming decades, not only in terrestrial systems but also in air and naval systems [1,2]. There are several potential advantages for using such a power source ranging from environmental to performance and operability aspects.

Among the various types of fuel cells currently available, due to their performance characteristics, Proton Exchange Membrane Fuel Cells (PEMFC), which work around 70 °C and with pressures close to atmospheric pressure, are at present the most suitable for use in transportation systems. Because

* Corresponding author.
E-mail address: gabrielcorrea.cba@gmail.com (G. Correa).
https://doi.org/10.1016/j.ijhydene.2017.09.169

the FCS dynamic response is relatively low, PEMFC-powered vehicles could be unstable at the sudden load change [3]. For vehicular use, these systems should be complemented by electrochemical energy storage devices, such as advanced rechargeable batteries, to guarantee the immediate delivery of the necessary power for the propulsion at any moment when required.

There are many motivations for introducing the hybridization in FCS for vehicular applications: decouple the fuel cell from the current demanded by the traction motor to allow the FCS to be used as close as possible to its optimum operating range. Energy recovery by decelerating and braking through regenerative brakes. Reduce FCS size and save the overall weight of the system. The transient FCS response observed in dynamic analysis is not instantaneous and typical transient phenomena such as overshoot effects can be visualized, that can be solved with the use of a complementary battery [4,5]. But the benefits are not limited to it, the use of a second source of energy could even work as an emergency power source, in the case of the failure of the fuel cell. On the other hand, the extra degree of freedom offered by the hybrid topology and the complex power flow, introduces the need for an energy management control strategy [6]. The Fuel Cell Hybrid Electric Vehicle (FCHEV) needs an Energy Management systems to distribute electrical power among the load and distinct power sources. The strategy must satisfy powertrain component constraints while trying to achieve some system-level performance objective such as maximizing fuel economy or maintaining the battery state-of-discharge (SoD).

In the specific literature, there are mainly two types of control approaches: rule-based and optimization-based [7]. Several studies have been performed on this technology, with the aim to attain improved performance and the contributions from the literature on FCHEV control techniques are numerous [8–16]. In the study done by Simmons [17], an on-board EMS with an optimal control based on Pontryagins Minimum Principle (PMP) is implemented to find the global optimal solution which minimizes fuel consumption. They developed a practical controller suitable for on-board implementation, in the form of an Auto-Regressive Moving Average (ARMA) regulator. Cipollone et al. [18] have proposed a method that considers a propulsion strategy where the fuel cell can be completely switched on or off, in order to achieve the best fuel cell efficiency. Many power management algorithms were designed by rule-based or heuristic methods. Those rule-based methods are simple and easy to understand because they come from engineering intuition [19,20]. However, they often lack optimality or cycle-beating. Ideally, fuel consumption minimization of hybrid vehicles can be achieved only when the driving scenario is known a priori. For instance, many authors implement online control through the Pontryagins Minimum Principle, but this method ensures optimality only when the driving cycle is known a priori. In particular, once the vehicle characteristics are defined, the optimal solution strictly depends on the speed trace and the total traveled distance [21–25]. Delprat and Bernard [26,27] develop the global optimization algorithm where the driving cycle needs to be a priori known.

In the present work, a full hybrid structure for a FCS/battery electric vehicle, with a lithium ion battery pack as secondary source is proposed. The FCS was selected as the main power supplier to minimize the usage of the battery. The dynamic behavior of a PEMFC system is a crucial factor to ensure the safe and effective operation of FCHEV [28]. Because water and thermal management are critical to stabilize the performance of the PEMFC during severe load changes, the model used in this work will include the fulfilled lumped capacitance model of the thermal management subsystem. This was developed to describe the temperature dynamics of the system based on the system inputs (power required and ambient temperature) [29]. Although in the FC the dynamic behavior of the Temperature is much slower than most of the electrochemical processes that take place inside the FC, the difference of H_2 consumptions between a stack model coupled to an accurate thermal model and a Model of FC without thermal is about 4%. The great majority of the research published on the subject carry out optimizations adopting static models that use polarization curves and efficiency tables [30,31]. As the performance of the hybrid vehicles (e.g., FCHEV) vary dramatically from driving patterns [32], in this work eight light duty vehicle driving cycles for urban, suburban and highway settings were considered: UDDS, LA92, NYCC, NEDC, HWFET, WLTP and CADC in its urban and rural road variants [33]. As the optimization process of the complex dynamic model requires a significant computational effort, simplified models were used to carry out the optimization process of each cycle, as shown in Fig. 1. A gradient-based method was employed to obtain the optimal energy management strategies, instead of methods such as PMP or DP, which cannot be used here because of the nature of the models.

These optimal strategies were used to train a particular NN for each cycle. Additionally, every NN was run over the rest of the cycles, showing different performances.

The aim of this paper is the development of an EMS capable of supervising the power flux from the fuel cell, obtaining a solution that minimizes the equivalent energy consumption of an a priori unknown cycle.

This work is organized as follows: in Section Vehicle model specifications and powertrain description a comprehensive description of the used vehicle parameters and the mathematical models of the vehicle, battery and the PEMFC systems is done. Also, a simplified model of the PEMFC is introduced to reduce the computational cost on the optimization stage. In Section Optimization method a minimization of the hydrogen consumption was carried out by the gradient-based method over the different driving cycles. Both the used algorithm and numerical results are also included in this section, showing the reliability of the obtained solutions. Section Neural network EMS describes the on-line control strategy based on neural networks as well as its training, using the ideal fuel cell power of Section Optimization method. Finally in Section Results, a quantitative and qualitative analysis of the behavior of the networks over the different types of cycles was made, classifying the administration strategies into two categories. Finally, it is shown the degree in which EMS improves the performance in terms of equivalent consumption by contrasting both the on-line neural network strategy and the ideal a priori known cycle optimization with the baseline case.

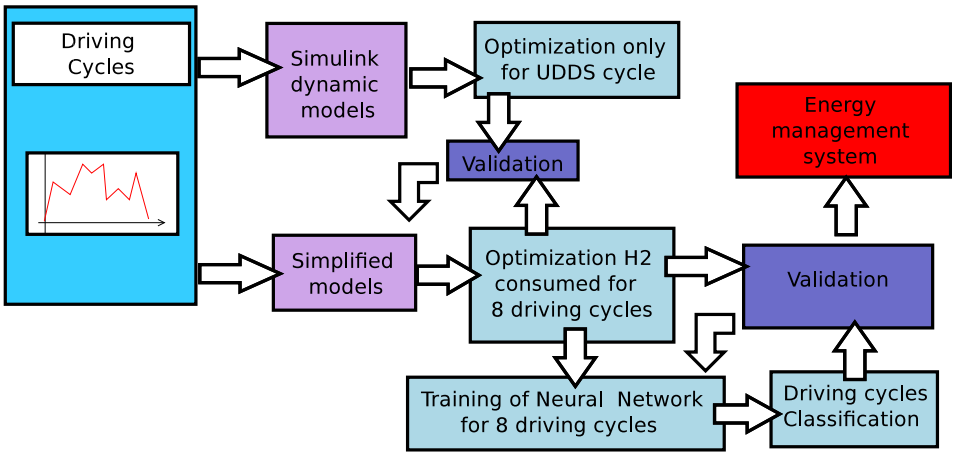

Fig. 1 – Work methods scheme.

Vehicle model specifications and powertrain description

The FCHEV powertrain architecture has a FCS with a battery functioning primarily as an auxiliary power unit. The battery and fuel cell supply electrical power to the electric traction motors through an electric bus balanced with two DC/DC converters. A schematic of the powertrain components specified is shown in Fig. 2.

Electronic and mechanical components efficiencies are assumed to be 0.97 and 0.85, respectively. Electric motor efficiency is given by the manufacturer as an efficiency map, which was integrated into the model. The vehicle dynamic model takes into account the gravitational forces, the aerodynamic drag, the rolling force and the acceleration forces. Eq. (1) shows how the requested electrical power is computed.

$$P_{req} = \frac{\left[\left(\frac{dV}{dt} + (f_0 + KV^2)\cos(\alpha) + g\sin(\alpha)\right)m + \frac{1}{2}C_D A\rho V^2\right]V}{\eta_{elec}\eta_{EC}\eta_{mec}} \quad (1)$$

Table 1 shows the vehicle specifications. Electric motor and the PEMFC stack maximum powers are 75 kW and 25 kW respectively. Capacity and initial value of SoD are 5 Ah and 30%, respectively.

Due to the electrochemical and thermal dynamic behavior of the FC, the power output differs significantly from that of the command signal. To ensure that the power delivered by the FC and the battery matches the electrical power requested by the driving cycle, the battery power request is defined as shown in Eq. (2).

$$P_{BAT} = P_{req} - P_{FC_{out}} \quad (2)$$

Fuel cell model

For this study, a PEMFC stack dynamic model derived from a past study [34,35] is used. This models take into account the FCS main electrochemical, fluid-dynamic and thermal properties in order to predict the power output with Matlab Simulink. The code is based on a FC stack dynamic model coupled with the model of the balance of plant, which includes compressor, cooling devices, and water management system. In order to obtain the cell voltage, the reactant pressures at the catalyst layer and the concentration as a function of the cells operating condition need to be calculated. Moreover, since the stack power output depends on the thermal systems, the temperature of the whole system needs to be computed (stack FC and water management

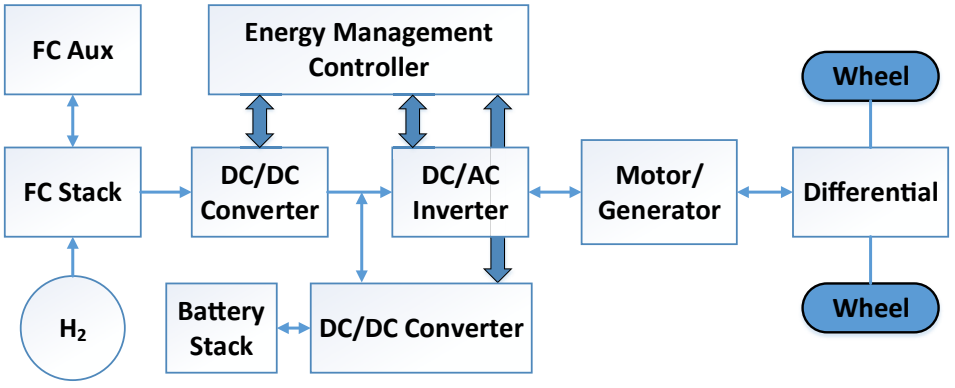

Fig. 2 – Schematic of the powertrain components.

Table 1 – Key parameters FCHEV.

Description	Parameter
Vehicle parameters	
Frontal area	1.9403 m^2
Coeff. rolling friction	0.013
K	6.51×10^{-6} s^2/m^2
Drag coefficient	0.35
Ambient temperature	298.15 K
Empty weight	754.4 kg
Total vehicle mass	1083 kg
PEMFC systems parameters	
Rated power	25 kW
Nº of cells	336
Purge hydrogen	1.2
Active area	200 cm^2
H_2 pressure	350 bar
H_2 storage weight	62.8 kg
FCS weight	103 kg
Electric motor parameters	
Continuous power	45
Continuous generator power	41
Peak torque	240 Nm
Peak power	75 kW
Battery parameters	
Rated capacity	5 Ah
Max. discharge current	150 A
Max. charge current	10 A
Nominal voltage	3.7 V
Cutoff voltage	2.7 V
Nº of cells	56
DOD	70
$SoD_{t=0}$	30%
Batteries weight	13 kg

system). The changes in temperature come from the production of heat by the exothermic chemical reaction, from internal heat dissipation, and from heat transfer with the cooling circuit.

The Nernst equation that gives the equilibrium voltage E_0 for a given reaction as a function of the temperature and the reactant pressures can be expressed as:

$$E_0 = -\frac{\Delta\bar{g}(T,p_0)}{2F} + \frac{RT_{st}}{2F}\ln\frac{P_{H_2}P_{O_2}^{0.5}}{P_{H_2O}} \quad (3)$$

As soon as a net current is produced by the fuel cell, the activation overvoltage (η_{act}), the concentration overvoltage (η_{conc}) and the ohmic overvoltage (η_{ohm}) take place in the cell. In Eq. (4), the actual cell voltage (V_{FC}) is obtained as the sum of the ideal Nernsts voltage (E) obtained from Eq. (3) and the overvoltages sum ($\sum\eta$).

$$V_{cell} = E_0 - \eta_{act} - \eta_{conc} - \eta_{ohm} \quad (4)$$

Given that the PEMFC is the primary source of energy, the aim of the EMS is to minimize the total hydrogen consumption, which is given by Eq. (5)

$$m_{H_2} = \int_{t_0}^{t_f} \frac{M_{H_2}}{N_C} 2F(I_{FC} + I_{aux})(t)dt, \quad (5)$$

where I_{FC} is the stack current, I_{aux} is the auxiliaries current, N_C is the number of cells in the stack and F is the Faraday constant (96485 C/mol). The model was validated on the basis of a through demonstration session performed in the framework of the ENFICA-FC project [36]. The validation of the model through experimental data is reported in Ref. [37]. Key equations of electrochemical, mass balance and thermal models are summarized in Table 2.

Battery model

The battery model is semi-empiric and quasi-static and takes into account the temperature effect as a variation in the battery voltage (ΔV) at a given temperature. It requires the charge and discharge curves of the battery voltage vs. SoD at different currents and the charge (Eq. (6)), as well as the discharge voltage change vs SoD curves at different temperatures (Eq. (7)). As functions of time, both, ambient temperature T_{amb} and the power required from the battery (Eq. (2)) are inputs to the model. The initial values of SoD and battery temperature are also required. The model parameters are given in Table 1.

The voltage and the current are obtained iteratively using the surface defined by the battery data (represented in Eq. (8)), in order to satisfy the condition that the voltage times the current is equal to the requested power. The iteration stops when the current reaches the limits defined by the manufacturer or the change in the current is less than 0.1 μA. If the voltage drops under the cut off voltage, the code stops and displays an error message. Once the working voltage and current are obtained, the temperature is defined by Eq. (9) and the SoD by Eq. (10). The battery losses are calculated as in Eq. (12) using the battery open circuit voltage (OCV) of Eq. (11) (obtained from the work [43]).

$$V_{@25^\circ C}(t) = f_1(SoD(t), I(t)) \quad (6)$$

$$\Delta V_T(t) = f_2(SoD(t), T_{bat}(t)) \quad (7)$$

$$V(t) = V_{@25^\circ C}(t) + \Delta V_T(t) \quad (8)$$

$$m_{bat}\cdot C_p\frac{dT(t)}{dt} = I(t)\cdot R - h_c\cdot A(T_{bat}(t) - T_{amb}(t)) \quad (9)$$

$$SoD(I(t),t) = SoD_{init} + \frac{1}{Cap}\int_0^t I(t)dt \quad (10)$$

$$V_{OC}(t) = f_1(SoD(t), 0) \quad (11)$$

$$P_{loss} = (V(t) - V_{OC}(t))\cdot I(t) \quad (12)$$

Fuel cell model simplification

The use of a complex dynamic model naturally requires a significant computational effort. Consequently, a simplified model is proposed in order to carry out the optimization process of each of cycle. It is important to note that every analyzed cycle takes over 1200 s to be solved using Simulink. In addition, the optimization process requires approximately 100 iterations until its convergence. That is why a method requiring low computational effort is proposed. As shown in Fig. 1, a simplified model of the FCS was made and the cycle

Table 2 – Key equations of electrochemical, mass balance and thermal model.

Description	Equation	Ref
Key equations of electrochemical model		
Activation loss at the electrodes	$\eta_{act_{cat}} + \eta_{act_{an}} = \eta_{act} = \frac{RT_{st}}{2F}\sinh^{-1}\left(\frac{i}{2i_{0,an}}\right) + \frac{RT_{st}}{0.5F}\sinh^{-1}\left(\frac{i}{2i_{0,ca}}\right)$	[38]
Cathode exchange current density	$i_{0,ca} = T^2(552\times10^{-9}) + T_{st}(-321\times10^{-6}) + 0.04674$	[34]
Ionic resistance	$r_{ion} = r_m = \frac{t_m}{(5.139\times10^{-9}\lambda_m - 3.26\times10^{-3})\exp\left(2416\left(\frac{1}{273}-\frac{1}{T_{st}}\right)\right)}$	[39]
Key equations of thermal model		
Change of energy rate	$mC_{st}\frac{dT_{st}}{dt} = \sum_i \pm G_i\cdot h_{ph,i} - \left\lvert\Phi_{conv}^{amb}\right\rvert - \left\lvert\Phi_{conv}^{WC}\right\rvert + \Phi_{source}$	
Heat convection to ambient	$\left\lvert\Phi_{conv}^{amb}\right\rvert = A_{st}^{amb}\cdot h_{conv}^{cell-amb}(T_{st} - T_{amb})$	[35]
Heat generation in the stack	$\Phi_{source} = nc\cdot i\cdot A_{cell}\left(\frac{-T_{st}\triangle\bar{s}}{2F} + \sum_j \eta_j\right)$	
Heat flux rate transfer to WC	$\left\lvert\Phi_{conv}^{WC}\right\rvert = A_{st}^{WC}\cdot h_{conv}^{WC-amb}(T_{st} - T_{WC})$	
Key equations of mass balance model		
Hydrogen effective partial pressure	$p_{H_2}^* = 0.5p_{H_2O}^{sat}\left[\frac{1}{x_{H_2O}^{channel}\exp\left(\frac{RT}{Pan2F}\frac{l_{st}l_{ca}}{D_{H_2O,H_2}}\right)}\right]$	[40] [41] [42]
Oxygen effective partial pressure	$p_{O_2}^* = p_{H_2O}^{sat}\left(\frac{1-x_{N_2}^*}{x_{H_2O}^*} - 1\right)$	

HWFET has been used as the test case for the autoregressive with exogenous terms (ARX) model validation with its Simulink model simulation.

$$A(q)y(t) = \sum_{i=1}^{n_u} B_i(q)u_i(t - n_{ki}) + e(t) \quad (13)$$

In Eq. (13), q is the forward shift operator, A and B_i are matrix valued polynomials in q (with orders n_a and n_b, respectively) that contain every model parameters identified so far. The model includes a process dead-time of n_k time-steps. For the present work, $n_a = 3$, $n_b = 3$ and $n_k = 0$, obtaining the following discrete-time ARX-model

$$A(z)y(t) = B(z)u(t) + e(t),$$

$$A(z) = 1 - 1.971z^{-1} + 1.023z^{-2} - 0.05225z^{-3},$$

$$B(z) = 6.973e^{-6} + 4.462e^{-7}z^{-1} + 6.26e^{-6}z^{-2}.$$

which was quadratically fitted.

In Fig. 3 is shown the outputs from the simplified and Simulink models.

Optimization method

In order to perform the minimization of the total energy consumption of the driving cycles described in the above section, some conditions shall be considered. First, a weighted function should be considered in order to achieve a low hydrogen consumption. Secondly, the state of discharge at the end of the cycle should be the same that at the beginning of the cycle, i.e., $SoD(t_0) = SoD(t_f)$. Finally, SoD must oscillate

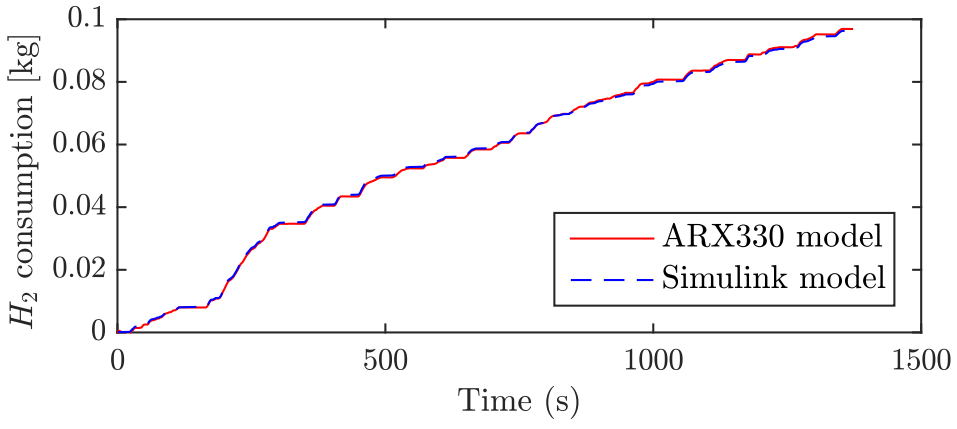

Fig. 3 – ARX model validation.

between 10 and 80 along the cycle. Then, taking $P_{FC}(t)$ as a variable, the cost function

$$m_{H_2} + \rho_0 W_0 + \rho_1 W_1 + \rho_2 W_2 \tag{14}$$

is minimized over all P_{FC} with $0 \le P_{FC}(t) \le 25$ kW for all t with $t_0 \le t \le t_f$, where

$$W_0 = \int_{t_0}^{t_f} max\{0, P_{BAT}(t)\}dt$$

is the energy discharged by the battery,

$$W_1 = \left(SoD(t_f) - SoD(t_0)\right)^2,$$

$$W_2 = \int_{t_0}^{t_f} \left(SoD(t) - \max\{10, \min\{SoD(t), 80\}\}\right)^2 dt$$

are the quadratic penalization for the violation of the SoD restrictions, and $\rho_0 > 0$, $\rho_1 > 0$, $\rho_2 > 0$ are properly chosen.

Method description

The models (simplified and Simulink) provides the m_{H_2} value and the $SoD(t)$ curve for a given power curve $P_{FC}(t)$ with $t_0 \le t \le t_f$. Thus, the exact derivative of the cost function (Eq. (14)) is not available. The Matlab built-in function *fmincon* and the Derivative Free Method BOBYQA [44] (using the NLopt library in Matlab) perform little progress on each iteration. This might be related to the low variation of the cost function. Hence, it is proposed to incorporate information of the curvature by using a quasi-Newton method. To be more specific, given a fixed time discretization $t_0 < t_1 < \ldots < t_f$, the values $P_{FC}(t_j)$ are obtained by minimizing at each iteration a quadratic approximation of the cost function subject to a box constraint. For the quadratic model, the gradient vector is computed with finite differences and the Hessian matrix is obtained by using the Broyden-Fletcher-Goldfarb-Shanno (BFGS) update with a Powell's correction, in order to guarantee a positive definite quadratic model (see Refs. [45,46]). For completeness, the method is described as follows. Let $\vec{\gamma}_*$ be the column vector with components $P_{FC}(t_j)$ and $\vec{\gamma}_k$ an approximation generated by the k-th iteration of the method. Let $\varphi(\vec{\gamma})$ be the value of the cost function (14) calculated using the components of $\vec{\gamma}$. In addition, let $\vec{\nu}_k$ be the column vector of variations of the cost function at each component of $\vec{\gamma}_k$. Hence, the following derivative-free box-constrained quasi-Newton method was used.

Choose $\sigma \in (0,1)$, $\kappa \in (0,1)$, $\vec{\gamma}_0$ and a matrix H_0. Compute $\vec{\nu}_0$. Set $k = 0$.

1. Compute $\vec{\zeta}_k$, solution of

$$\underset{\vec{\zeta}}{\text{minimize}} \quad (\vec{\nu}_k)^T \vec{\zeta} + \frac{1}{2}\vec{\zeta}^T H_k \vec{\zeta}$$

$$\text{subject to} \quad 0 \le \left(\vec{\gamma}_k + \vec{\zeta}\right)_j \le 25, \quad j = 0, \ldots, f.$$

2. Perform a backtracking to find $\alpha_k \in (0,1]$ satisfying the Armijo condition

$$\varphi\left(\vec{\gamma}_k + \alpha_k \vec{\zeta}_k\right) \le \varphi(\vec{\gamma}_k) + \sigma\alpha_k (\vec{\nu}_k)^T \zeta_k$$

3. Set $\vec{\gamma}_{k+1} = \vec{\gamma}_k + \alpha_k \vec{\zeta}_k$ and compute $\vec{\nu}_{k+1}$.
4. If $\|\vec{\gamma}_{k+1} - \max\{0, \min\{\vec{\gamma}_{k+1} - \vec{\nu}_{k+1}, 25\}\}\| < tol$, STOP.
5. Set $\vec{\delta} = \vec{\gamma}_{k+1} - \vec{\gamma}_k$, $\vec{\mu} = \vec{\nu}_{k+1} - \vec{\nu}_k$ and $\tau = (\vec{\delta})^T H_k \vec{\delta}$.
   If $(\vec{\delta})^T \vec{\mu} < \kappa\tau$, set $\vec{\mu} = \theta\vec{\mu} + (1-\theta) H_k \vec{\delta}$ for $\theta = (1-\kappa)\frac{\tau}{\tau - (\vec{\delta})^T \vec{\mu}}$.

   Define

$$H_{k+1} = H_k - \frac{H_k \vec{\delta} \left(H_k \vec{\delta}\right)^T}{\tau} + \frac{\vec{\mu}(\vec{\mu})^T}{(\vec{\delta})^T \vec{\mu}}$$

6. Set $k = k + 1$ and go to Step 1.

The vector $\vec{\gamma}_*$ was set as the approximate vector satisfying the condition in Step 4. This algorithm was implemented in Matlab and, in this work, the weights for the cost function (14) were $\rho_0 = 1/3600$ and $\rho_1 = \rho_2 = 1$, and the algorithmic parameters values were $\sigma = 10^{-4}$ and $\kappa = 0.2$. Since each evaluation of the cost function requires the execution of the models, the calculation of finite differences in Step 3 is a time-consuming operation. Nevertheless, this algorithm was able to solve the problem unlike fmincon or BOBYQA. In order to solve the time-consumption of the Simulink model, the simplified models explained in Subsection Fuel cell model simplification were used.

Optimization results

The optimization procedure was performed over the 8 cycles. Those results are shown in Fig. 4 by drawing the frequency of the power delivered by each power source. Table 3 shows the result and analysis of the energy consumed, produced and exchanged between the sources. The cycle energy required refers to the electrical energy requested by the car to the power sources. FCS energy supplied to the system is the net energy output of the FCS, which includes the FCS energy supplied to the battery. Battery energy supplied to the system is the net energy output of the battery. Available break energy is the energy that the generator is able to harvest from breaking after electronic losses. Due to power peaks, not all of this energy is delivered to the battery, thus the net break energy is the break energy that is actually used to charge the battery after battery charging losses. The battery energy loss includes losses due to charge and discharge processes. Finally, the net energy delivered to the battery is the sum of the energies delivered by the FCS and the generator to the battery.

In Fig. 5 a comparison between the value of the cost function at the optimal strategy (red bars) and at a baseline case (blue bars) is shown. The baseline case used is the trivial energy management where the fuel cell power is selected as the primary source and therefore always works to provide the required power, when the FC can not provide the necessary power the battery delivers the rest of the power required. It can be seen that in almost all of the cycles, the cost function value decreases substantially obtaining decreases up to 2% of the baseline cost in the CADC cycles, except in the cycle NEDC where the optimal cost is 96% of the baseline cost. In this cycle, the baseline case is very close to the optimum case.

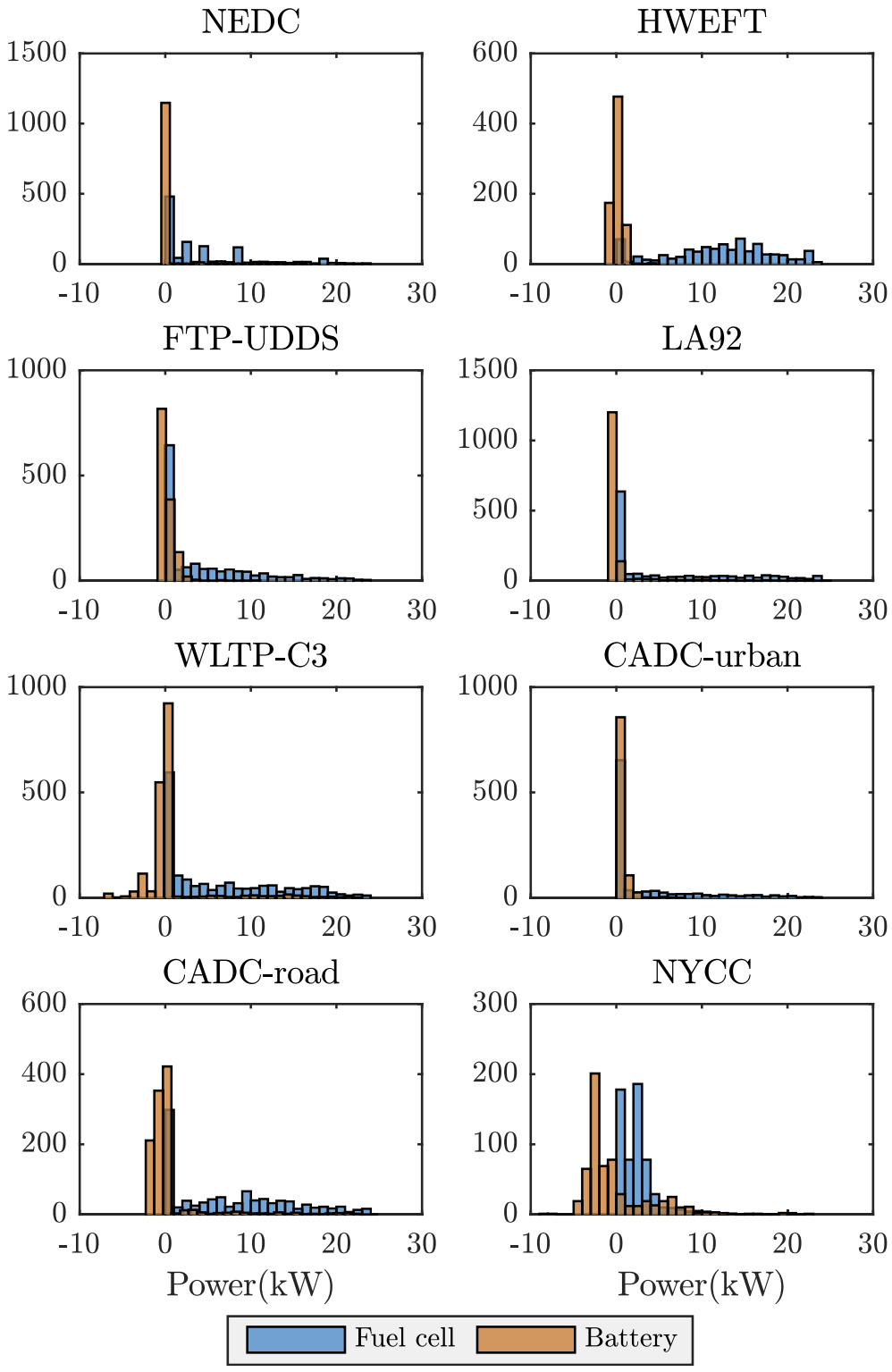

Fig. 4 – Optimal case power frequencies.

Neural network EMS

This section will show how to approximate the global optimized $P_{FC}(t)$ of the last section via a real-time management energy algorithm based on Neural Networks.

Every cycle is associated to a particular NARX[1] neural network consisting in 2 layers[2] of 10 neurons and 7 backward

[1] Nonlinear autoregressive exogenous model.
[2] One of them is hidden.

Table 3 – Optimal energy management data summary.

	NEDC	HWEFT	UDDS	LA92	WLTP	CADCu	CADCr	NYCC
Cycle required energy [kWh]	1.71	2.59	1.83	3.05	4.19	0.96	2.81	0.37
FCS energy supplied to system [kWh]	1.63	2.57	1.71	2.95	3.99	0.88	2.76	0.36
FC energy supplied to battery [kWh]	0.02	0.00	0.01	0.06	0.25	0.00	0.16	0.14
Battery energy supplied to system [kWh]	0.10	0.03	0.15	0.21	0.47	0.12	0.26	0.17
Available break energy [kWh]	0.15	0.07	0.25	0.43	0.33	0.21	0.28	0.08
Net break energy [kWh]	0.09	0.03	0.14	0.16	0.12	0.12	0.13	0.05
Battery energy loss [kWh]	0.01	0.00	0.01	0.02	0.06	0.01	0.04	0.02
Net energy delivered to battery [kWh]	0.11	0.03	0.15	0.22	0.37	0.12	0.29	0.19
FCS energy delivered to system	94%	99%	92%	93%	89%	88%	91%	67%
Battery energy delivered to system	6%	1%	8%	7%	11%	12%	9%	33%
Brake energy delivered to battery	61%	44%	56%	37%	36%	56%	46%	64%
Brake energy loss	39%	56%	44%	63%	64%	44%	54%	36%
Battery charge from braking	85%	97%	94%	73%	32%	98%	45%	26%
Battery charge from FCS	15%	3%	6%	27%	68%	2%	55%	74%

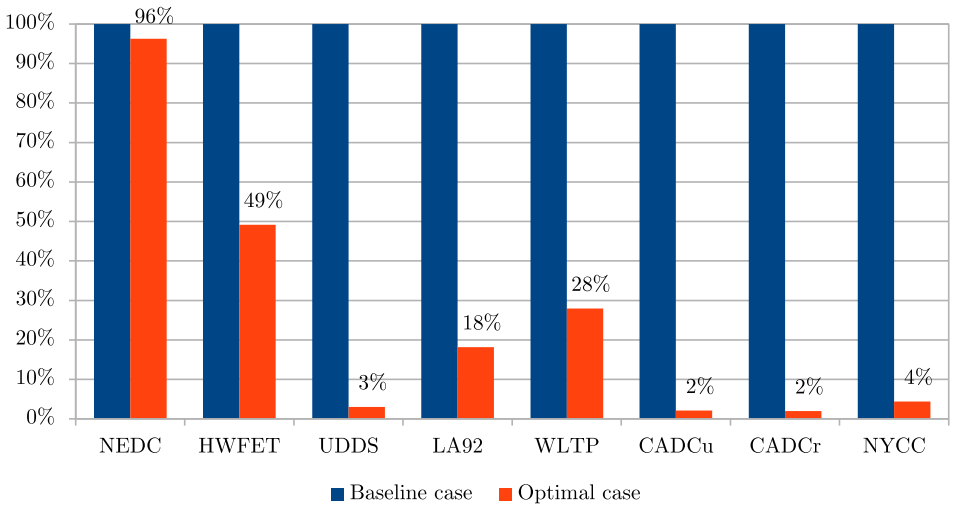

Fig. 5 – Cost function result.

time steps [47]. The neural network of the cycle is trained in order to predict the fuel cell power $P_{FC}(t)$ from

$$P_{FC}(t-\Delta t),\ldots,P_{FC}(t-7\Delta t) \tag{15}$$

and the electrical required total power

$$\vec{P}_{req}=\left(P_{req}(t),P_{req}(t-\Delta t),\ldots,P_{req}(t-6\Delta t)\right). \tag{16}$$

Note that the advanced in time $P_{req}(t)$ is considered available, as usual. Additionally, the wheel brake power (P_{wb})

$$\vec{P}_{wb}=\left(P_{wb}(t),P_{wb}(t-\Delta t),\ldots,P_{wb}(t-6\Delta t)\right) \tag{17}$$

and the integrals

$$\int^{t}\vec{P}_{req}dt \text{ and } \int^{t}\vec{P}_{wb}dt \tag{18}$$

were also incorporated as inputs.

Once the neural network is trained, the control strategy (see Fig. 6) consists in computing an approximation $\widehat{P}_{FC}(t)$ of $P_{FC}(t)$ that will be the network output, taking as past values of the fuel cell power

$$\widehat{P}_{FC}(t-\Delta t),\ldots,\widehat{P}_{FC}(t-7\Delta t),$$

in place of Eq. (15). This way, $\widehat{P}_{FC}(t)$ is calculated from its 7 recently computed last values, which is always mathematically possible if rest initial conditions are assumed. Matlab neural networks toolbox was used for the training, by using a Levenberg-Marquardt method to compute the weights and biases, and hyperbolic tangent type sigmoid and linear functions for the transfer function of the hidden and output layers, respectively (see Supplementary material).

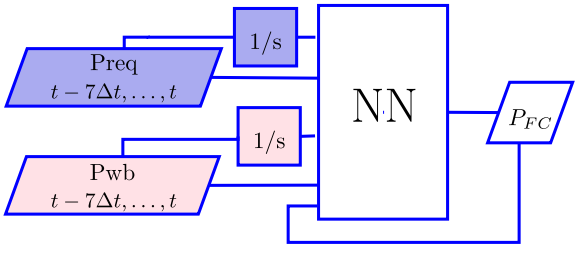

Fig. 6 – Neural Network control block diagram.

The introduction of $\overrightarrow{P}_{wb}$ and the integrals of Eq. (18) as inputs played a very important role here. Actually, not only this substantially reduced the prediction error, but also made some cycles networks to be capable to predict the fuel cell power of *other different cycles*. Once the eight neural strategies were computed, they were subsequently also tested at every cycle, besides their particular ones, in order to study the performance of every *network vs cycle* possible combination.

Obviously, the required electrical power will in general have a strong dependence of the driving cycle (Fig. 4) and consequently, any kind of general control strategy is in principle hard to be imagined. Nevertheless, the mere existence of groups of cycles having at glance similar features in principle suggests that there could be just a few of common neural control strategies, able to predict the whole set of cycles power requirements. This is exactly what is studied in detail in the following section.

Results

In order to study the performance of the EMS, the equivalent consumption (19) will be used.

$$r = \frac{|SoD_f - SoD_0|BSE}{\eta_{FC}100} + m_{H_2}LHV \tag{19}$$

This index measures the energy in kWh consumed by the model. The second term of Eq. (19) is clearly related with the H_2 consumed from the tank. The term of the absolute difference between the initial and final SoDs may be interpreted as a kind of deviation from the most idealistic case, in which there is neither useless savings $(SoD_f > SoD_0)$ nor need of recharging $(SoD_f < SoD_0)$ of energy, in what respects to the battery usage. Eq. (20) gives the relative error of the equivalent consumption of the j-th cycle obtained with the i-th neural strategy $(\widehat{r}_{ij})$, and the optimal equivalent consumption of the j-th cycle (r_j).

$$M_{ij} = \frac{|\widehat{r}_{ij} - r_j|}{r_j} \tag{20}$$

The index was used to assess the performances of the 64 possible combination of EMS and cycles and the results are shown in Fig. 7. The cells of the table are colored in a linear gradient according with the values, green being the best valuation, red the worst, and yellow the middle point. The white blocks represent the cases in which the EMS leads to the battery depletion and the cycle was not finished.

Cycles driving classification

From Fig. 7 one can infer the existence of a partial crossing cycle prediction capability. Hence, it is proposed to classify the driving cycles into only two categories, mainly *urban* group and mainly *interurban and highway* group. As shown in Fig. 7, HWFET neural strategy run over HWFET turns out to have the minimum relative error 0.25%. On the other hand, the maximum relative error was obtained when CADC road was run over NYCC 104.65%. However, without taking into account NYCC (since the cycle optimum is difficult to be reproduced by the proposed EMS), the maximum relative error was obtained when CADC road was run over CADC urban (73.33%), followed by HWFET run over CADC urban (71.04%). The mean relative error of every neural strategy applied to the other cycles was 20.44%, and without taking into account NYCC, it was 15%. According to these results, neural strategies trained with aggressive cycles (e.g., CADC urban) should in general work for every cycle. In contrast, soft cycles neural strategies (e.g., HWFET or NEDC) may not work with aggressive cycles. While the choice of driving cycles always has an impact on the performance of vehicles, certain types of driving cycles amplify this impact in hybrid and electric vehicle powertrains. While hybrid and plug-in vehicles offer little economy consumption benefit at higher costs for highway driving (HWFET), they can offer dramatic fuel reductions and costs savings in aggressive driving with frequent stops and idling [32]. As can be seen in Fig. 7 the neural strategy trained with the CADC urban shows the best performance when used with unknown driving cycles. In contrast, the neural strategy trained with the NYCC can only be used in the NYCC. This behavior can be explained looking at Fig. 4 and Table 3, where the battery is frequently charged (negative power) by both the regenerative brake (26%) and the fuel cell (74%). The EMS provided by this cycle, where the battery energy supply is the largest, may explain why this strategy depletes the battery in the rest of the cycles. On the other hand, one can see on Fig. 7 that the neural strategy trained by the highway driving cycle HWFET has its worst performance when applied to the strongly urban cycles NYCC, CADC urban, LA92 and UDDS. The EMS trained with the CADC urban cycle achieves the lowest mean error, for urban cycles UDDS, LA92, CADC urban and NYCC and getting worse for highway cycles (e.g. HWFET). Besides, the EMS trained with the HWFET shows good results for interurban cycles such us NEDC, HWFET, WLTP, and CADC road. From this analysis, it is clear that a natural cycle classification into two groups can be made: urban cycles that includes UDDS, LA92, CADC urban and NYCC cycles, and interurban and highway cycles that

	NEDC	HWFET	UDDS	LA92	WLTP	CADCu	CADCr	NYCC
NEDC	0.51%	1.30%	4.25%	4.96%	2.22%	23.46%	5.33%	34.69%
HWFET	**1.37%**	**0.25%**	38.35%	-	**0.52%**	71.04%	**3.47%**	57.78%
UDDS	0.69%	4.55%	0.84%	-	-	29.15%	-	40.77%
LA92	16.80%	10.40%	28.96%	0.51%	0.98%	41.94%	1.41%	52.02%
WLTP	4.79%	2.04%	19.35%	28.49%	0.64%	52.76%	4.56%	76.05%
CADCu	4.76%	32.35%	**1.98%**	**4.80%**	7.84%	**2.20%**	8.35%	**8.40%**
CADCr	46.10%	23.82%	45.64%	-	2.62%	73.33%	0.37%	104.65%
NYCC	-	-	-	-	-	-	-	28.57%

Fig. 7 – Relative error of the equivalent consumption between the optimal case and the EMS response. The bold font is used to indicate the energy management strategy used for each cycle.

includes NEDC, HWFET, WLTP, and CADC road cycles. As it can be seen in Fig. 8, good results can be obtained with the EMS trained with the CADC urban applied to the urban cycles and the EMS trained with the HWFET cycle applied to the interurban and highway cycles.

Comparative results

In order to visualize in a more quantitative and qualitative way the above results, it is convenient to show more specifically in which degree EMS improves the performance in terms of equivalent consumption (see (20)), for instance by contrasting both the on-line neural network strategy and the ideal a priori known cycle optimization with the baseline case. This is summarized in Table 4 and Fig. 9.

In Fig. 9 the equivalent consumption per km (in $g \cdot km^{-1}$) for the baseline case is represented by the blue bars. The yellow bars corresponds to the case of the control designed with the neural networks of Section Neural network EMS, and the red bars shows the results of the equivalent consumption given by Section Optimization method, in which the optimization is done in the most idealistic case when the cycles are known a

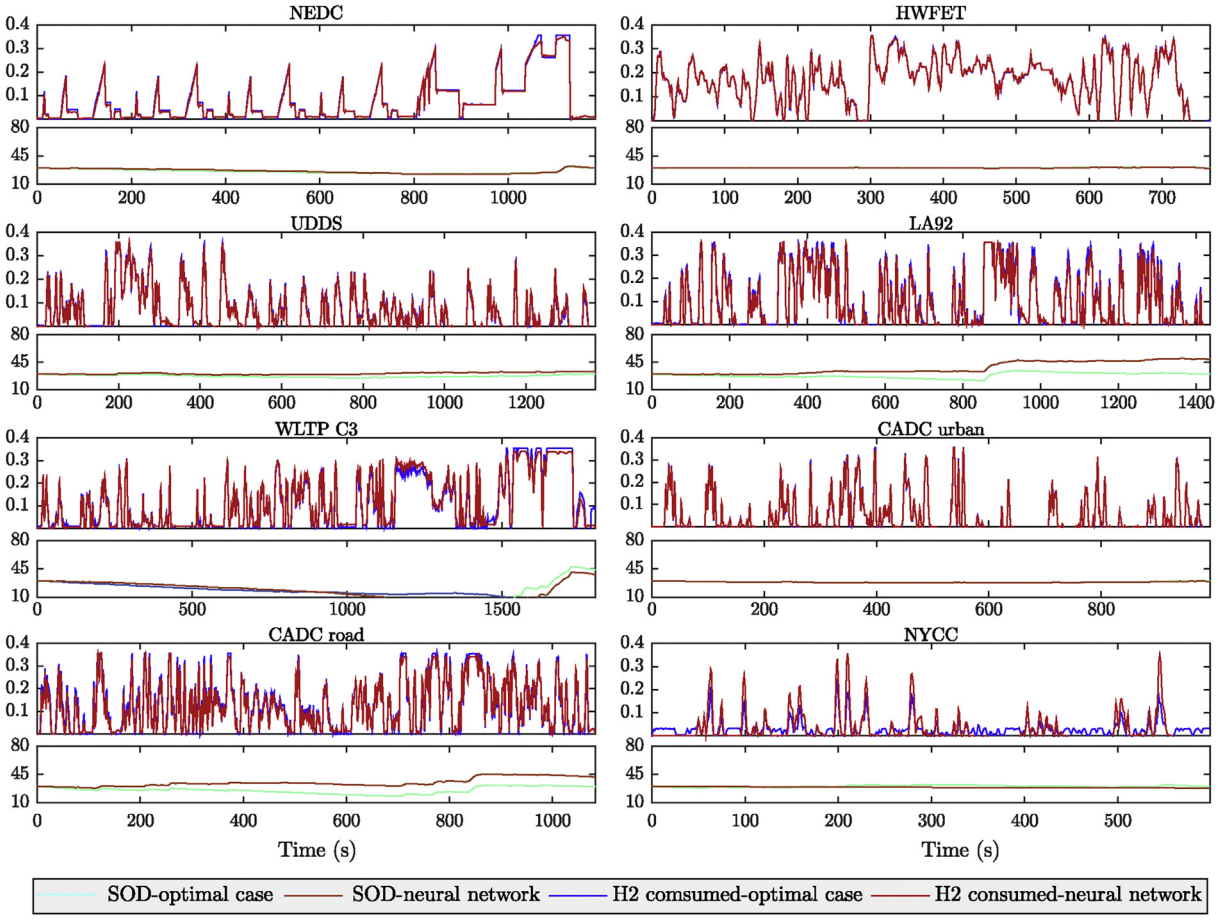

Fig. 8 – Hydrogen flow (g/s) and SoD for the optimal case and EMS energy management.

Table 4 – H_2 consumed - SOD for baseline case, Optimal case and Estrategy based on NN.

	NEDC	HWEFT	UDDS	LA92	WLTP	CADCu	CADCr	NYCC
Baseline case								
H_2 consumed [kg]	0.084	0.132	0.092	0.147	0.192	0.050	0.133	0.019
Final SoD	29.681	27.883	20.411	34.746	57.320	21.563	45.359	26.355
Equivalent consumption [g/km]	0.254	0.270	0.277	0.318	0.307	0.387	0.279	0.390
Optimal case								
H_2 consumed [kg]	0.084	0.131	0.087	0.150	0.203	0.045	0.141	0.018
Final SoD	30.009	30.009	30.009	30.009	43.876	30.009	30.010	29.997
Equivalent consumption savings [%]	0.52	2.05	12.80	0.69	0.05	19.79	2.27	17.76
Estrategy based on NN								
H_2 consumed [kg]	0.083	0.131	0.087	0.150	0.202	0.046	0.142	0.021
Final SoD	30.754	29.769	29.534	29.519	46.252	29.471	30.538	27.335
Equivalent consumption savings [%]	−0.84	1.80	11.07	−4.07	0.57	18.03	−1.12	10.85

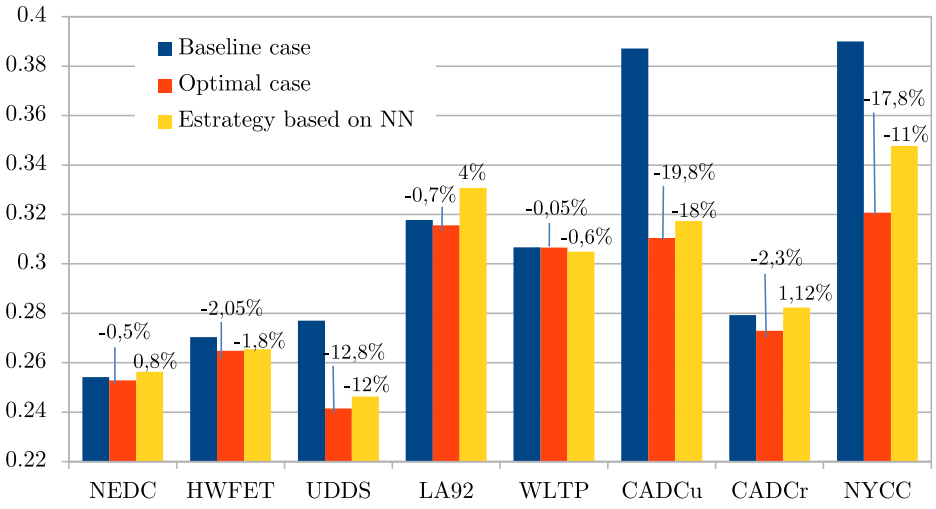

Fig. 9 – Comparison of equivalent consumption per km (g/km) and percentage difference with respect to the baseline.

priori. The equivalent consumption percentage difference against the baseline case is shown on top of each bar.

In most of the cycles, the NN strategy either reduces the consumption with respect to the baseline case or produces an overall result that is close to the optimal performance. For the cycles in which the optimal and baseline strategies are approximately comparable, the NN strategy in general produces similar results (e.g. NEDC, LA92 and CADC road), improving in some cases the performance (e.g. HWEFT, WLTP). For the cycles UDDS, CADC urban and NYCC, in which the optimal consumption is clearly lower than the baseline case, the NN strategy also reduces the consumption, being sometimes very close to the optimal scenario (e.g. UDDS, CADC urban). The urban EMS applied to the urban cycles obtains an overall improvement close to 10%: 12% in the UDDS, 18% in the CADC urban and 11% in the NYCC. On the other hand, when applied to the LA92, the urban EMS shows no improvement, which can be explained due to the fact that the optimal case is very close to the baseline case. For the intercity and highway EMS the later observation applies, obtaining improvements of 1.8% for the HWFET and 0.6% for the WLTP.

Conclusion

In this work, a new online EMS controller that manages the power fluxes of a FCHEV power sources was introduced using dynamical models and neural networks. The dynamic models of the vehicle with its particular power sources ensure an improved EMS design because they take into account several factors that cannot be included by the use of static models (e.g. the maximum current of battery charge, working temperature, etc.). Eight neural networks were created and trained with inputs provided by optimizing simplified models, which have been used in order to reduce the highly computational cost of the optimization with Simulink models. The use of neural networks provides a real-time EMS. The robustness of this method was provided by running each neural strategy over the rest of the cycles, increasing the reliability to predict unknown cycles. With this methodology, a quantitative and qualitative analysis was made, showing the behavior of the networks over different type of cycles. From this analysis the administration strategies can be classified into two categories that cover most of the possible driving styles types: *urban* and *interurban and highway*. The results show that using the proposed methodology it is possible to obtain this two suitable EMS to be implemented in a real-time vehicle controller. For a highway and intercity driving style the NN trained with the HWFET cycle has the best performance showing energy equivalent savings up to 2% whereas the NN trained with the CADC urban cycle achieves the lowest mean error for urban cycles obtain the energy equivalent savings up to 18%.

Acknowledgements

This work was partially supported by the project PICT 2014 No 2534 and the project PIO No 15920150100001CO. The authors acknowledge the contribution of CONICET-UNCA, MINCyT and the FCEFyN-UNC Aeronautical Department.

Appendix A. Supplementary data

Supplementary data related to this article can be found at https://doi.org/10.1016/j.ijhydene.2017.09.169.

Symbols

Latin symbols

A	Area [m^2]
A_{cell}	Cell active surface [cm^2]
E_0	Open Circuit Voltage [V]
F	Faraday number [C/mol]
g	Gibbs free energy [W]
G	Mass flow rate [kg/s]

h	Mass specific enthalpy of the mass flow [J/kg]
i	Current density [A/cm^2]
I	Current [A]
m	Mass [kg]
N_c	Number of cells in series in the PEMFC stack
p	Pressure [bar]
P	Power [kW]
r	Resistance [Ω m^2]
R	Universal gas constant [J/(mol K)]
t_m	Membrane thickness [cm]
T	Temperature [K]

Greek symbols

Φ	Heat transfer [W]
η	over-voltage [V]
ρ	Air density [kg/m^3]
δ_m	Membrane average water content
$\Delta\bar{s}$	Molar entropy of the reaction [J/molK]

Abbreviations and acronyms

act	Activation
amb	Ambient
an	Anode
ca	Cathode
Mem	Membrane
ohm	Ohmic
st	Stack
ADS	Average driving speed
BSE	Battery system energy
DOD	Depth of discharge
DP	Dynamic programming
EMS	Energy management system
FC	Fuel cell
FCHEV	Fuel Cell Hybrid Electric Vehicle
FCS	Fuel Cell System
PEMFC	Proton Exchange Membrane Fuel Cells
PKE	Positive kinetic energy

REFERENCES

[1] Sohn S-I, Oh J-H, Lee Y-S, Park D-H, Oh I-K. Design of a fuel-cell-powered catamaran-type unmanned surface vehicle. IEEE J Ocean Eng 2015;40(2):388–96. https://doi.org/10.1109/JOE.2014.2315889.

[2] Romeo G, Borello F, Correa G. Setup and test flights of all-electric two-seater aeroplane powered by fuel cells. J Aircr 2011;48(4):1331–41. https://doi.org/10.2514/1.C031271.

[3] Wang Y, Chen KS, Mishler J, Cho SC, Adroher XC. A review of polymer electrolyte membrane fuel cells: technology, applications, and needs on fundamental research. Appl Energy 2011;88(4):981–1007. https://doi.org/10.1016/j.apenergy.2010.09.030.

[4] Jang J-H, Yan W-M, Chiu H-C, Lui J-Y. Dynamic cell performance of kW-grade proton exchange membrane fuel cell stack with dead-ended anode. Appl Energy 2015;142:108–14. https://doi.org/10.1016/j.apenergy.2014.12.073.

[5] Tang Y, Yuan W, Pan M, Li Z, Chen G, Li Y. Experimental investigation of dynamic performance and transient responses of a kW-class PEM fuel cell stack under various load changes. Appl Energy 2010;87(4):1410–7. https://doi.org/10.1016/j.apenergy.2009.08.047.

[6] Chen Z, Xiong R, Wang C, Cao J. An on-line predictive energy management strategy for plug-in hybrid electric vehicles to counter the uncertain prediction of the driving cycle. Appl Energy 2017;185:1663–72. https://doi.org/10.1016/j.apenergy.2016.01.071.

[7] Sulaiman N, Hannan M, Mohamed A, Majlan E, Wan Daud W. A review on energy management system for fuel cell hybrid electric vehicle: issues and challenges. Renew Sustain Energy Rev 2015;52:802–14. https://doi.org/10.1016/j.rser.2015.07.132.

[8] Ettihir K, Boulon L, Agbossou K. Optimization-based energy management strategy for a fuel cell/battery hybrid power system. Appl Energy 2016;163:142–53. https://doi.org/10.1016/j.apenergy.2015.10.176. http://linkinghub.elsevier.com/retrieve/pii/S030626191501418X.

[9] Kim MJ, Peng H. Power management and design optimization of fuel cell/battery hybrid vehicles. J Power Sources 2007;165(2):819–32. https://doi.org/10.1016/j.jpowsour.2006.12.038.

[10] Song Z, Li J, Han X, Xu L, Lu L, Ouyang M, et al. Multi-objective optimization of a semi-active battery/supercapacitor energy storage system for electric vehicles. Appl Energy 2014;135:212–24. https://doi.org/10.1016/j.apenergy.2014.06.087.

[11] Xie C, Ogden JM, Quan S, Chen Q. Optimal power management for fuel cell-battery full hybrid powertrain on a test station. Int J Electr Power Energy Syst 2013;53(1):307–20. https://doi.org/10.1016/j.ijepes.2013.05.016.

[12] Xu L, Ouyang M, Li J, Yang F. Dynamic Programming Algorithm for minimizing operating cost of a PEM fuel cell vehicle. Ind Electron (ISIE) 2012:1490–5. 2012 IEEE International Symposium on.

[13] Ravey A, Roche R, Blunier B, Miraoui A. Combined optimal sizing and energy management of hybrid electric vehicles. In: 2012 IEEE Transportation Electrification Conference and Expo (ITEC), no. 5. IEEE; 2012. p. 1–6. https://doi.org/10.1109/ITEC.2012.6243420. http://ieeexplore.ieee.org/lpdocs/epic03/wrapper.htm?arnumber=6243420.

[14] Hu X, Murgovski N, Johannesson L, Egardt B. Energy efficiency analysis of a series plug-in hybrid electric bus with different energy management strategies and battery sizes. Appl Energy 2013;111:1001–9. https://doi.org/10.1016/j.apenergy.2013.06.056.

[15] Barelli L, Bidini G, Ottaviano A. Optimization of a PEMFC/battery pack power system for a bus application. Appl Energy 2012;97:777–84. https://doi.org/10.1016/j.apenergy.2011.11.043.

[16] Fares D, Chedid R, Panik F, Karaki S, Jabr R. Dynamic programming technique for optimizing fuel cell hybrid vehicles. Int J Hydrogen Energy 2015;40(24):7777–90. https://doi.org/10.1016/j.ijhydene.2014.12.120. http://www.sciencedirect.com/science/article/pii/S0360319914035526.

[17] Simmons K, Guezennec Y, Onori S. Modeling and energy management control design for a fuel cell hybrid. J Power Sources 2014;246:736–46.

[18] Cipollone R, Di Battista D, Marchionni M, Villante C. Model based design and optimization of a fuel cell electric vehicle. Energy Procedia 2014;45:71–80. https://doi.org/10.1016/j.egypro.2014.01.009.

[19] Ahmadi S, Bathaee S. Multi-objective genetic optimization of the fuel cell hybrid vehicle supervisory system: fuzzy logic and operating mode control strategies. Int J Hydrogen Energy 2015;40(36):12512–21. https://doi.org/10.1016/j.ijhydene.2015.06.160. http://www.sciencedirect.com/science/article/pii/S0360319915016894.

[20] Xu G, Li W, Xu K, Song Z. An intelligent regenerative braking strategy for electric vehicles. Energies 2011;4(9):1461–77. https://doi.org/10.3390/en4091461.

[21] Chen Z, Mi CC, Xia B, You C. Energy management of power-split plug-in hybrid electric vehicles based on simulated annealing and Pontryagin's minimum principle. J Power Sources 2014;272:160–8. https://doi.org/10.1016/j.jpowsour.2014.08.057. http://www.sciencedirect.com/science/article/pii/S0378775314013123.
[22] Xu L, Ouyang M, Li J, Yang F, Lu L, Hua J. Application of Pontryagin's Minimal Principle to the energy management strategy of plugin fuel cell electric vehicles. Int J Hydrogen Energy 2013;38(24):10104–15. https://doi.org/10.1016/j.ijhydene.2013.05.125.
[23] Zheng CH, Kim NW, Park YI, Lim WS, Cha SW, Xu GQ. The effect of battery temperature on total fuel consumption of fuel cell hybrid vehicles. Int J Hydrogen Energy 2013;38(13):5192–200. https://doi.org/10.1016/j.ijhydene.2013.02.048.
[24] Liu C, Liu L. Optimal power source sizing of fuel cell hybrid vehicles based on Pontryagin's minimum principle. Int J Hydrogen Energy 2015;40(26):8454–64. https://doi.org/10.1016/j.ijhydene.2015.04.112.
[25] Ettihir K, Higuita Cano M, Boulon L, Agbossou K. Design of an adaptive EMS for fuel cell vehicles. Int J Hydrogen Energy 2017;42(2):1481–9. https://doi.org/10.1016/j.ijhydene.2016.07.211. http://www.sciencedirect.com/science/article/pii/S0360319916306929.
[26] Bernard J, Delprat S, Buechi F, Guerra T. Global optimisation in the power management of a fuel cell hybrid vehicle (FCHV). In: 2006 IEEE vehicle power and propulsion conference. IEEE; 2006. p. 1–6. https://doi.org/10.1109/VPPC.2006.364289. http://ieeexplore.ieee.org/document/4211317/.
[27] Delprat S, Lauber J, Guerra T, Rimaux J. Control of a parallel hybrid powertrain: optimal control. IEEE Trans Veh Technol 2004;53(3):872–81. https://doi.org/10.1109/TVT.2004.827161. http://ieeexplore.ieee.org/document/1300877/.
[28] Kang S, Min K. Dynamic simulation of a fuel cell hybrid vehicle during the federal test procedure-75 driving cycle. Appl Energy 2016;161:181–96. https://doi.org/10.1016/j.apenergy.2015.09.093.
[29] Correa G, Borello F, Santarelli M. Sensitivity analysis of temperature uncertainty in an aircraft PEM fuel cell. Int J Hydrogen Energy 2011;36(22):14745–58. https://doi.org/10.1016/j.ijhydene.2011.08.036. http://linkinghub.elsevier.com/retrieve/pii/S0360319911019239.
[30] Feroldi D, Serra M, Riera J. Energy management strategies based on efficiency map for fuel cell hybrid vehicles. J Power Sources 2009;190(2):387–401. https://doi.org/10.1016/j.jpowsour.2009.01.040.
[31] Sorrentino M, Pianese C, Maiorino M. An integrated mathematical tool aimed at developing highly performing and cost-effective fuel cell hybrid vehicles. J Power Sources 2013;221(221):308–17. https://doi.org/10.1016/j.jpowsour.2012.08.001. http://linkinghub.elsevier.com/retrieve/pii/S0378775312012591.
[32] Karabasoglu O, Michalek J. Influence of driving patterns on life cycle cost and emissions of hybrid and plug-in electric vehicle powertrains. Energy Policy 2013;60:445–61. https://doi.org/10.1016/j.enpol.2013.03.047.
[33] T Barlow, S Latham, I Mccrae, P Boulter, A reference book of driving cycles for use in the measurement of road vehicle emissions. TRL Published Project Report. https://doi.org/10.1108/WJSTSD-06-2014-0009.
[34] Correa G, Santarelli M, Borello F, Cestino E, Romeo G. Flight test validation of the dynamic model of a fuel cell system for ultra-light aircraft. Proc Inst Mech Eng Part G J Aerosp Eng 2015;229(5):917–32. https://doi.org/10.1177/0954410014541081. http://pig.sagepub.com/lookup/doi/10.1177/0954410014541081.
[35] Correa G, Borello F, Santarelli M. Sensitivity analysis of stack power uncertainty in a PEMFC-based powertrain for aircraft application. Int J Hydrogen Energy 2015;40(32):10354–65. https://doi.org/10.1016/j.ijhydene.2015.05.133. http://www.scopus.com/inward/record.url?eid=2-s2.0-84937523800{\&}partnerID=tZOtx3y1.
[36] Romeo G, Borello F, Correa G, Cestino E. ENFICA-FC: design of transport aircraft powered by fuel cell & flight test of zero emission 2-seater aircraft powered by fuel cells fueled by hydrogen. Int J Hydrogen Energy 2013;38(1):469–79. https://doi.org/10.1016/j.ijhydene.2012.09.064. http://linkinghub.elsevier.com/retrieve/pii/S0360319912021027.
[37] Romeo G, Correa G, Borello F, Cestino E, Santarelli M. Air cooling of a two-seater fuel cell powered aircraft: dynamic modeling and comparison with experimental data. J Aerosp Eng 2012;25(3):356–68. https://doi.org/10.1061/(ASCE)AS.1943-5525.0000138.
[38] Santarelli M, Torchio M, Cochis P. Parameters estimation of a PEM fuel cell polarization curve and analysis of their behavior with temperature. J Power Sources 2006;159(2):824–35. https://doi.org/10.1016/j.jpowsour.2005.11.099. http://www.scopus.com/inward/record.url?eid=2-s2.0-33748032089{\&}partnerID=tZOtx3y1.
[39] Zawodzinski T, Neeman M, Sillerud LO, Gottesfeld S. Determination of water diffusion coefficients in perfluorosulfonate ionomeric membranes. J Phys Chem 1991;95:6040.
[40] Amphlett JC, Mann RF, Peppley BA, Thurgood CP. Application of ButlerVolmer equations in the modelling of activation polarization for PEM fuel cells. J Power Sources 2006;161:775–81.
[41] Amphlett JC, Baumert RM, Mann RF, Peppley BA, Roberge PR. Performance modeling of the Ballard Mark IV solid polymer electrolyte fuel cell, I. Mechanistic model development. J Electrochem Soc 1995;142(1):1–8.
[42] Springer T, Zawodzinski T, Gottesfeld S. Polymer electrolyte fuel cell model. J Electrochem Soc 1991;138:2334–41.
[43] Truchot C, Dubarry M, Liaw BY. State-of-charge estimation and uncertainty for lithium-ion battery strings. Appl Energy 2014;119:218–27. https://doi.org/10.1016/j.apenergy.2013.12.046.
[44] MJ Powell, The bobyqa algorithm for bound constrained optimization without derivatives, Cambridge NA Report NA2009/06, University of Cambridge: Cambridge.
[45] Bertsekas DP. Nonlinear programming. Athena Scientific; 1999.
[46] Bonnans J-F, Gilbert JC, Lemaréchal C, Sagastizábal CA. Numerical optimization: theoretical and practical aspects. Springer Science & Business Media; 2006.
[47] Siegelmann H, Horne B, Lee Giles C. Computational capabilities of recurrent NARX neural networks. IEEE Trans Syst Man, Cybern Part B Cybern 1997;27(2):208–15.